http://dx.doi.org/10.21577/0103-5053.20190195

J. Braz. Chem. Soc., Vol. 30, No. 12, 2681-2690, 2019
Printed in Brazil - ©2019 Sociedade Brasileira de Química

Article

Nanoparticles of Fe_2O_3 and Co_3O_4 as Efficient Electrocatalysts for Oxygen Reduction Reaction in Acid Medium

Ismael C. B. Alves,[a] José R. N. Santos,[a] Deracilde S. S. Viégas,[a] Edmar P. Marques,[b] Cristina A. Lacerda,[b] Lei Zhang,[a,c,d] Jiujun Zhang[a,c] and Aldaléa L. B. Marques[,a]

[a]*Núcleo de Estudos em Petróleo e Energia (NEPE), Laboratório de Pesquisa em Química Analítica (LPQA) and Laboratório de Análises e Pesquisa em Química Analítica de Petróleo e Biocombustíveis (LAPQAP), Departamento de Tecnologia Química, Universidade Federal do Maranhão (UFMA), 65080-805 São Luís-MA, Brazil*

[b]*Departamento de Química, Universidade Federal do Maranhão (UFMA), 65080-805 São Luís-MA, Brazil*

[c]*Institute for Sustainable Energy, College of Sciences, Shanghai University, 200444 Shanghai, China*

[d]*Energy, Mining & Environment, National Research Council of Canada, BC V6T 1W5 Vancouver, BC, Canada*

This paper presents a comparative study about the oxygen reduction reaction (ORR) catalyzed by nanoparticles of Fe_2O_3 and Co_3O_4 applied on the surface of glassy carbon electrodes (GCE). The nanoparticles were synthesized using the modified polymeric precursor method (Pechini). These two nanomaterials were characterized by Fourier transform infrared spectroscopy (FTIR) and X-ray diffraction (XRD) techniques. The estimated average particle sizes were 21 and 31 nm for Fe_2O_3 and Co_3O_4, respectively. Electrochemical impedance spectroscopy (EIS) showed that Fe_2O_3/GCE has lower charge transfer resistance than Co_3O_4/GCE. The surface electrochemistry of both Fe_2O_3/GCE and Co_3O_4/GCE was studied in the solution free of O_2, and their corresponding reaction mechanisms were analyzed. The electrocatalytic ORR activities of these two catalysts were studied by cyclic voltammetry (CV) and rotating disk electrode (RDE) in acidic solution. The results obtained by RDE indicated that both Fe_2O_3/GCE and Co_3O_4/GCE can catalyze the ORR with a dominating 2-electron transfer process to produce H_2O_2, using a potential of −0.8 V. These kinetic results indicate that Fe_2O_3/GCE is more efficient than Co_3O_4/GCE in terms of ORR. Considering the low cost of these two non-noble metal catalysts, they may be used as viable alternatives for ORR electrocatalysts.

Keywords: electrocatalysis, metallic nanoparticles, iron oxide, cobalt oxide, oxygen reduction

Introduction

In electrochemical energy storage and conversion devices such as fuel cell and metal-air batteries, the applications of electrocatalysts for cathode oxygen reduction reaction (ORR) are of paramount importance.[1,2] As recognized, ORR in aqueous solutions occurs mainly through two pathways: one is the direct 4-electron reduction from O_2 to water (H_2O), and the other is the 2-electron reduction from O_2 to hydrogen peroxide (H_2O_2). In general, the ORR kinetics on electrodes is sluggish. To speed up this reaction for a practical operation, electrocatalysts are necessary. Normally, platinum (Pt) and its alloys are used as electrocatalysts for ORR. However, Pt is expensive hindering its large-scale commercialization in electrochemical conversion technologies such as fuel cells and metal-air batteries.[3] Thus, researchers have made great efforts to replace Pt-based catalysts with non-precious metal ones for enabling the practical application of the technologies, and these metals have been considered for both, cathode[4-6] and anode of fuel cells.[7-9] Regarding non-precious metal electrocatalysts, many types have been explored, including metal oxides, organometallic complexes, and so on.[10]

*e-mail: aldalea.ufma@hotmail.com

Among non-precious metal oxide materials, iron (Fe) and cobalt (Co) oxides have been extensively investigated as electrocatalysts for ORR. For example, Wu *et al.*[11] synthesized iron oxide (Fe_3O_4) nanoparticles supported on nitrogen-doped graphene airgel (Fe_3O_4/N-GAs), and found its high catalytic activity towards ORR, and claimed that their catalyst had an even higher durability than the commercial Pt/C. Chen *et al.*[12] reported that a nanostructured cobalt oxide (Co_3O_4) supported on hollow carbon spheres (Co_3O_4/HCS) was an efficient catalyst for ORR in basic media. Recently, iron oxide nanoparticles in different phases (Fe_3O_4, γ-Fe_2O_3, α-Fe_2O_3 and α-FeOOH) forming a composite with reduced graphene oxide aerogels,[13] and cobalt oxide with nitrogen-doped graphene (Co-N/G),[14] were used as electrocatalysts, showing good catalytic ORR performance.

The synthesis method can significantly influence the sizes of nanoparticles, and this is a determinant factor in the electrocatalytic ORR performance. The existing methods, such as sol-gel,[15] liquid combustion,[16] spraydrying,[17,18] hydrothermal[19,20] and the polymeric precursor are proved to be efficient. Among them, the polymeric precursor method, also called Pechini,[21-23] stands out as a promising technique for the preparation of crystalline and nanometric metal oxides with controlled particle sizes. Actually, to our best knowledge, there is no work yet found for using this polymeric precursor method to synthesize ORR electrocatalysts, which is why we have chosen this method to synthesize the catalysts in this paper.

In this paper, we have synthesized nanoparticles of iron and cobalt oxides (Fe_2O_3 and Co_3O_4) using the polymeric precursors method and explored their catalytic ORR performance in acidic medium. The synthesized catalysts were characterized using the techniques of Fourier transform infrared spectroscopy (FTIR) and X-ray diffraction (XRD). The electrocatalytic ORR activity of the catalyst-modified electrodes was evaluated by cyclic voltammetry (CV), linear scanning voltammetry (LSV), and rotational disk electrode (RDE). The electrochemical impedance spectroscopy (EIS) was also used to analyze the electron/mass transfer resistances related to the catalytic ORR process.

Experimental

Reagents

All reagents used in this work were analytical grade and used without further purification. Cobalt(II) chloride hexahydrate, iron(II) chloride tetrahydrate, citric acid, ethylene glycol, boric acid, sodium perchlorate monohydrate, and sodium hydroxide were all purchased from Merck (Darmstadt, Germany). Sulfuric acid and Nafion® were purchased from Sigma-Aldrich (Saint Louis, USA), acetic acid and phosphoric acid were purchased from Vetec (Saint Louis, USA). The study of pH influence on the electrochemical response was performed using the Britton-Robson (BR) buffer prepared in the usual way, i.e., by mixing solutions of phosphoric acid, acetic acid and boric acid, all 0.04 mol L^{-1}, whose solution had a pH close to 1.8. An appropriate amount of 2 mol L^{-1} sodium hydroxide solution was added dropwise to the solution to adjust the pH as desired. All solutions were prepared using deionized water (18 MΩ cm resistance), purified by a Milli-Q system (Millipore Inc., USA).

Synthesis of nanoparticles of iron and cobalt oxides

The nanoparticles of the metal oxides (Fe_2O_3 and Co_3O_4) were synthesized by the polymeric precursor method. First, 7.0 g of the metal precursor (cobalt(II) chloride hexahydrate or iron(II) chloride tetrahydrate) were added to 50 mL of water under constant stirring at 80 °C until the complete dissolution of the salt. Then citric acid (20.29 g for cobalt(II) chloride hexahydrate solution, or 16.96 g for iron(II) tetrahydrate chloride solution) was added with a mole ratio of metal to acid of 1:3 for the formation of metal citrate solution. The temperature was then raised to 120 °C, and ethylene glycol (12.18 g for cobalt(II) chloride hexahydrate solution, or 10.18 mL for iron(II) chloride tetrahydrate solution) was added in a ratio of the ethylene glycol to metal of 60:40 (%m/m) for polymerization to occur. The obtained gel was dried in an oven (ca. 100 °C) for 24 h to remove excess water. After the procedure above, the obtained material was subjected to a calcination process at a temperature of 300 °C for 2 h to form the puff, which was ground, and again calcined at 500 °C for 2 h for obtaining the metal oxides.[21-23]

Modification of working electrode and electrochemical measurements

For the modification of the glassy carbon electrode (GCE) with the catalysts, a suspension at the concentration of 3.0×10^{-3} mol L^{-1} of catalyst nanoparticles (Fe_2O_3 or Co_3O_4) in deionized water with 1% of Nafion® was prepared under ultrasonication for 5 min at room temperature. Prior to modification, the GCE surface was buffed with alumina and rinsed with deionized water. After cleaning, a 15 μL aliquot of the catalyst suspension was deposited onto the GCE surface, and then the modified electrode was taken to the desiccator for vacuum drying. The catalyst loadings for both Fe_2O_3 or Co_3O_4 were approximately 6.43×10^{-4} mmol cm^{-2}.

The electrochemical experiments were performed using a potentiostat model PGSTAT 302 from Metrohm-Autolab. A conventional three-electrode cell containing the catalyst-modified disk GCE with a geometric surface (A_{geom}) of 0.07 cm^2 as the working electrode was employed for both the cyclic voltammetry and rotating disk electrode experiments. $Ag_{(s)}|Cl_{(s)}|Cl^-$ (KCl_{sat}) was used as the reference electrode and a platinum wire as the counter electrode. For the measurements with rotating disk electrode, a controller of rotation from Autolab (motor controller) was used.

The O_2-saturated standard solution was produced by bubbling double distilled water with pure O_2 at room temperature for 1 h. The O_2 content in the O_2 saturated water was taken as 1.21×10^{-3} mol L^{-1}, calculated as recommended by the literature.[24-26] The electrochemical measurements were carried out in a 25 mL cell with 10 mL solutions which were purged with pure nitrogen and kept under nitrogen atmosphere at room temperature.

Results and Discussion

Physical-chemical characterization of the catalysts

Infrared spectra (FTIR) of the synthesized catalyst materials (Fe_2O_3 and Co_3O_4) were recorded on a Shimadzu IR Prestige-21 spectrometer in the wavenumber region of 400 to 4000 cm^{-1}. The test samples were prepared in KBr pellets (1%). The XRD analysis was performed using a Bruker D8 Advance diffractometer using Cu Kα radiation in the 2θ angle range between 10 and 80°.

Figure 1 shows the infrared spectra obtained in the region of 400 to 4000 cm^{-1} for Fe_2O_3 and Co_3O_4 samples, respectively. The spectrum obtained for Fe_2O_3 shows intense bands at 452 and 551 cm^{-1}, which are related to the transverse stretching vibrations of Fe–O.[27,28] The weak band at 1050 cm^{-1} can be attributed to hematite,[29] and the one at 2345 cm^{-1} can be attributed to air CO_2. Similar behavior was observed by Eigler *et al.*[30] For Co_3O_4, the bands at 567 and 665 cm^{-1} are related to the Co–O stretching vibrations. The presence of these bands supports the formation of the Co_3O_4 spinel network. The band at 567 cm^{-1} corresponds to the stretching of the Co^{3+}–O bond, while the band at 665 cm^{-1} can be attributed to the Co^{2+}–O stretching vibration. These assignments are in accordance with the literature,[31,32] thus confirming the formation of metallic spinel structure.

XRD analysis was performed to investigate the phase and structure of the synthesized catalyst materials. The diffractogram obtained for iron oxide (Figure 2) shows the diffraction peaks at 2θ of 24.2°, 30.2°, 35.6°, 41°, 49.5°, 54.1°, 57.5°, 62.4°, and 64.1°, corresponding to

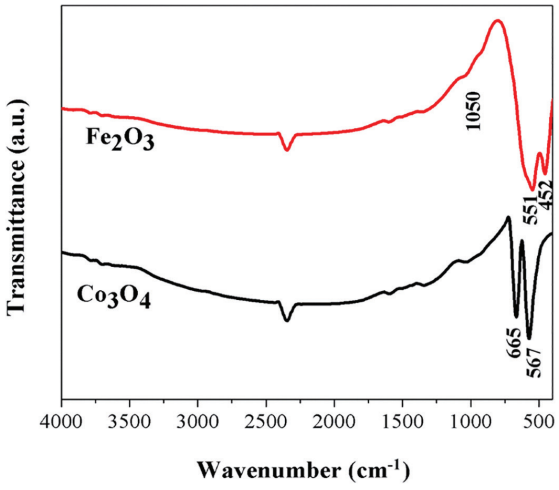

Figure 1. FTIR spectra (KBr) of the Fe_2O_3 and Co_3O_4 samples.

the planes 012, 104, 110, 113, 024, 116, 018, 214, and 300, respectively, for α-Fe_2O_3 nanoparticles, which can be easily indexed to their hexagonal phase, as reported by Mirzaei *et al.*[21] The peak at 2θ of 43° is assigned to plane 400 of magnetite (Fe_3O_4).[33-35] Cobalt oxide (Figure 2) exhibits peaks at 2θ 19.1°; 31.3°; 36.8°; 38.5°; 44.9°; 55.7°; 59.4°; 65.2°; referring to planes 111, 220, 311, 222, 400, 422, 511, and 440, respectively.[36,37] The positions of these peaks can be indexed to Co_3O_4 structure in cubic spinel. This phase is characteristic of the cubic face centered structure, which coincides with that presented by Gunnewiek *et al.*[22] The format of the diffractogram coincides with those reported in previous works.[37,38]

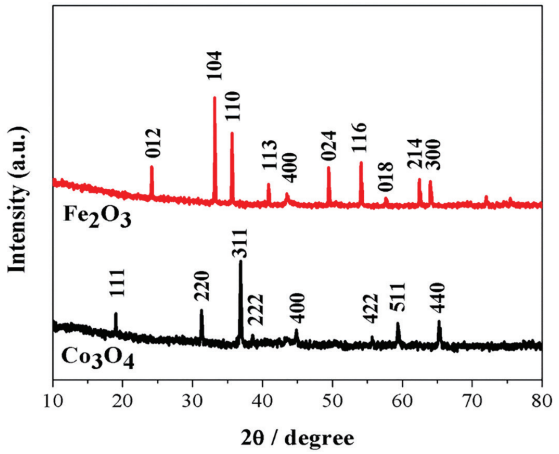

Figure 2. Diffractograms of Fe_2O_3 and Co_3O_4 catalyst samples.

The crystallite dimensions were estimated by applying the Scherrer method[39] (equation 1) to the diffractograms shown in Figure 2.

$$d = \frac{0.9\lambda}{\beta \cos\theta} \quad (1)$$

where d is the size of the crystallites (nm), λ is the wavelength of the Cu Kα radiation (0.154 nm), β is the width at half height in radians, and θ is the Bragg angle in the plane relative to the peak. The average sizes of the calculated crystallites are approximately 21 and 31 nm for the nanoparticles of Fe_2O_3 and Co_3O_4, respectively. These results show the efficiency of the method in synthesizing the nanoparticles of the catalysts. Compared with those reported in literature, the catalyst nanoparticle sizes are smaller: Gunnewiek *et al.*[22] obtained Co_3O_4 nanoparticles with a mean diameter of 36 nm, and Mirzaei *et al.*[21] obtained an approximate value of 70 nm for α-Fe_2O_3. Compared with the sample obtained by hydrothermal method, the nanoparticle sizes of α-Fe_2O_3 crystallites were 45-65 nm, which are larger than ours. Sahoo and Satpati[31] also used the hydrothermal method and obtained Co_3O_4 nanoparticles with a mean size of 50 nm. All these results above show that the polymeric precursor method is more efficient in obtaining nanoparticles with smaller sizes.

Electrochemical behavior of GCE modified with Fe_2O_3 and Co_3O_4

Figure 3a shows the cyclic voltammograms of GCEs modified with Fe_2O_3 and Co_3O_4, respectively, recorded between −0.8 and 0.9 V *vs.* $Ag_{(s)}|Cl_{(s)}|Cl^-$ (KCl_{sat}), in BR buffer pH 1.8, saturated with N_2. For comparison, those results with bare GCE are also displayed in the figure.

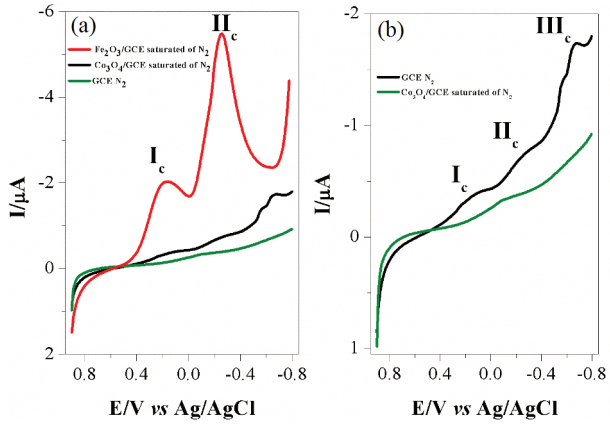

Figure 3. (a) Linear scanning voltammograms (LSV) obtained in 0.1 mol L^{-1} BR buffer (pH 1.8) saturated with N_2 at GCE (olive-green line), Fe_2O_3/GCE (red line) and Co_3O_4/GCE (black line) with a catalyst loading of 0.643 mg cm^{-2}; (b) GCE (olive-green line) and Co_3O_4/GCE (black line). Potential scan rate: 20 mV s^{-1}. The scan directions for all curves are from left to right.

In Figure 3a, there is no significant redox process observed on the unmodified GCE electrode. Note that there is a small reduction wave around −0.1 V, which comes from the C=O group on the carbon surface. For Fe_2O_3/GCE, two cathodic peaks can be observed, which are marked as: I_c and II_c, located at 0.21 and −0.255 V *vs.* Ag/AgCl, respectively. By referring to literature[40,41] these peaks can be proposed to the following two reactions:

Reaction I_c at 0.21 V: $Fe_2O_3 + 2H^+ + 2e^- \rightarrow 2FeO + H_2O$ (2)

Reaction II_c at −0.255 V: $FeO + 2e^- + 2H^+ \rightarrow Fe + H_2O$ (3)

Figure 3b shows the enlarged voltammogram of only Co_3O_4/GCE from Figure 3a, in which three processes marked as I_c, II_c and III_c can be clearly observed. These three redox processes may be assigned to equations 4, 5 and 6, respectively, by referring to the literature[42,43] for acidic redox processes of Co_3O_4. Actually, Co_3O_4 is a mixed oxide containing CoO and Co_2O_3, which can be expressed as $CoO.Co_2O_3$. The process I_c at 0.143 V may be assigned to Co^{3+}/Co^{2+} according to equation 4. The process II_c at −0.261 V refers to Co^{2+}/Co^{+} redox reaction expressed by equation 5. The process III_c at −0.66 V may be assigned to the redox reaction of Co^{+}/Co^{0}.

Reaction I_c at 0.143 V: $Co_2O_3 + 2H^+ + 2e^- \rightarrow 2CoO + H_2O$ (4)

Reaction II_c at −0.261 V: $2CoO + 2H^+ + 2e^- \rightarrow Co_2O + H_2O$ (5)

Reaction III_c at −0.66 V: $Co_2O + 2H^+ + 2e^- \rightarrow 2Co + H_2O$ (6)

Electrocatalytic ORR performance of both Fe_2O_3/GCE and Co_3O_4/GCE

Figure 4 shows the cyclic voltammograms (CVs) of GCE, Fe_2O_3/GCE and Co_3O_4/GCE in BR buffer pH 1.8 saturated by oxygen (1.3×10^{-3} mol L^{-1}). For comparison, cyclic voltammograms in the absence of oxygen were also recorded. It can be seen that, although the unmodified GCE shows an insignificant ORR activity in the presence of oxygen, the electrode modified with Fe_2O_3 or Co_3O_4 gives significantly enhanced ORR current, demonstrating that both Fe_2O_3 and Co_3O_4 have strong catalytic ORR activities. The current densities obtained in this experiment for ORR by Fe_2O_3/GCE and Co_3O_4/GCE were 40 and 30 μA, respectively, showing that the modification with iron oxide presents a significant increase in current densities. For Fe_2O_3/GCE, the electrocatalytic process occurs close to the redox response of Fe^{3+} (peak II_c), indicating that the

Fe^{2+} metal center is responsible for the electrocatalytic process of ORR. Wu *et al.*[11] obtained similar behavior using Fe oxide nanoparticles supported on graphene. For the Co_3O_4/GCE, the process occurs near the peak III_c, which corresponds to Co^{3+}/Co^{2+}, indicating that this Co^{2+} metal center is responsible for the electrocatalytic ORR activity. This result is similar to that reported by Chen *et al.*[12]

From Figure 4, it can also be observed that, under the same conditions, Fe_2O_3/GCE can give higher ORR than Co_3O_4/GCE. For this phenomenon may have contributed two factors, one is the higher intrinsic catalytic ORR activity of the former than the latter, and the second is the size effect of the catalyst nanoparticles. The average size of Fe_2O_3 particles is smaller than that of Co_3O_4, as analyzed by diffractograms in Figure 2. The small-sized Fe_2O_3 can have a larger contact surface, therefore, a higher catalytic current can be expected.[44,45]

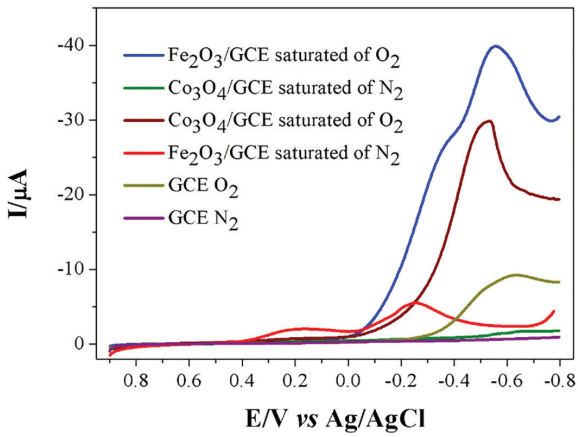

Figure 4. Cyclic voltammograms of GCE, Fe_2O_3/GCE and Co_3O_4/GCE in the presence of N_2 and O_2. Purple curve: GCE N_2; dark yellow curve: GCE O_2; red curve: Fe_2O_3/GCE in 0.1 mol L^{-1} BR buffer pH 1.8 saturated with N_2; blue curve: Fe_2O_3/GCE in O_2-saturated solution; green curve: Co_3O_4/GCE in N_2-saturated solution; brown curve: Co_3O_4/GCE in O_2-saturated solution. Potential scan rate: 20 mV s^{-1}.

Effect of potential scanning rate on ORR activity

Figure 5 shows the linear sweep voltammograms obtained at different potential rates from 5 to 500 mV s^{-1} in O_2-saturated solution for oxygen reduction with individually Fe_2O_3 and Co_3O_4 modified GCE in BR buffer solution (pH 1.8). The voltammetric peak currents corresponding to the irreversible ORR process vary

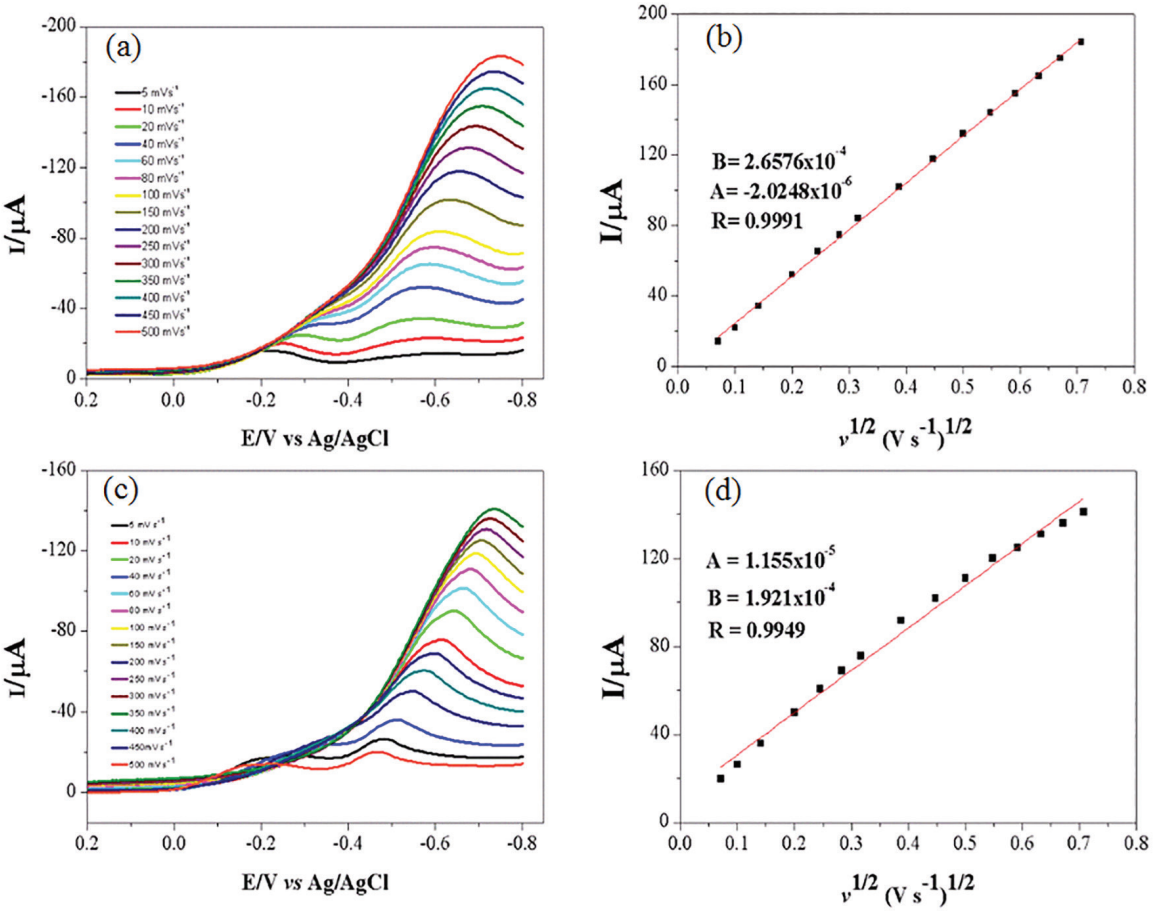

Figure 5. (a) Linear sweep voltammetry (LSV) curves of ORR on Fe_2O_3/GCE obtained in 0.1 mol L^{-1} BR buffer pH 1.8 saturated with O_2 at different potential scan rates (5 to 500 mV s^{-1}); (b) I_p *versus* $v^{1/2}$ for Fe_2O_3/GCE; (c) ORR LSV on Co_3O_4/GCE at different scan rates; (d) I_p *versus* $v^{1/2}$ for Co_3O_4/GCE.

linearly with the square root of the potential scan rate (Figures 5b and 5d) for both Fe_2O_3/GCE and Co_3O_4/GCE. This behavior suggests that the ORR catalyzed by these two catalysts is controlled by diffusion of the solution oxygen to the electrode surface.[46]

Electrochemical impedance spectroscopy

Figure 6 shows the Nyquist plots obtained by electrochemical impedance spectroscopy for Fe_2O_3/GCE (Figure 6a) and Co_3O_4/GCE (Figure 6b) in oxygen-saturated BR buffer solution (pH 1.8), respectively. The cell potential was controlled at −0.5 V *vs.* Ag|AgCl in the frequency range of 100 mHz to 100 kHz.

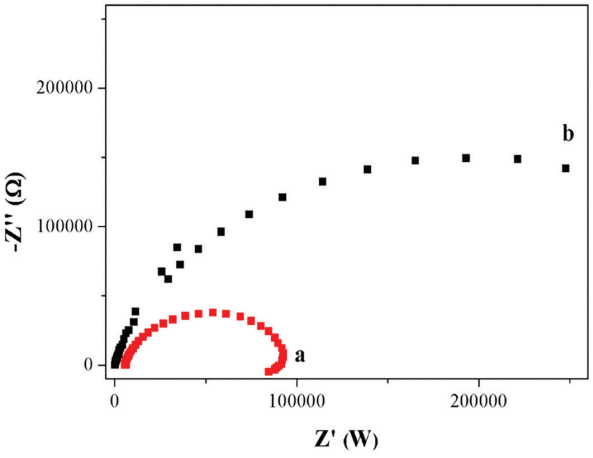

Figure 6. Nyquist plots for Fe_2O_3/GCE (a) and Co_3O_4/GCE (b) in the presence of saturating O_2 at a controlled potential of −0.5 V *vs.* Ag/AgCl in the frequency range of 100 mHz to 100 kHz with an amplitude of 0.005 rms.

The plots shown in Figure 6 consist of typical semicircles,[47] which represent the ORR charge transfer resistances. The smaller the size of the semicircle, the faster the charge transfer kinetics of the catalyzed ORR.[48-50] Therefore, the catalytic ORR activity of Fe_2O_3/GCE is higher than that of Co_3O_4/GCE. This result is in consistence with those observed in Figures 4 and 5. Further quantitative measurements will be presented in the following sections.

Measurements on Fe_2O_3 and Co_3O_4 modified rotating disc electrodes

The steady-state LSV curves were recorded at different rotational rates (rpm) of Fe_2O_3 and Co_3O_4 modified rotating disc electrodes (RDEs); the results are shown in Figure 7a for Fe_2O_3/GCE and Figure 7b for Co_3O_4/GCE, respectively. It can be observed that, with increasing rotation rate, the ORR currents are increased. The ORR current density (I) on the RDE can be expressed as equation 7 according to Koutecky-Levich.[51]

$$\frac{1}{I} = \frac{1}{I_k} + \frac{1}{I_d} \quad (7)$$

where I is the measured current density, I_k represents the kinetic current density (absence of any mass transport effect) and I_d is the limit diffusional current density, defined by the following equation 8:

$$I_d = B\,\omega^{1/2} = (0.201\ n\ F\ A\ D_o^{2/3}\ C_o\ v^{-1/6})\ \omega^{1/2} \quad (8)$$

where n is the number of electrons involved in the ORR *per* O_2, F is the Faraday constant (96487 C mol^{-1}), A is the electrode area (0.07 cm^2), D_o is the diffusion coefficient (1.93×10^{-5} cm^2 s^{-1}), C_o is the solubility of O_2 in the solution (1.21×10^{-6} mol cm^{-3} taken from literature), v is the kinematic viscosity of the solution (1.01×10^{-2} cm^2 s^{-1}), and ω is the rotation rate of the electrode in rpm.

The graph of I_d^{-1} *versus* $\omega^{-1/2}$, according to equation 8, allows to estimate the apparent number of electrons transferred (n) for the electrocatalytic ORR. Figures 7b and 7d show the Koutecky-Levich plots at the −0.8 V potential for Fe_2O_3/GCE and Co_3O_4/GCE, respectively, and the theoretical plots for 2- and 4-electron processes in the ORR process are also shown for comparison. According to the slopes obtained, the average ORR electron number calculated for Fe_2O_3/GCE is n = 1.8, and for Co_3O_4/GCE is n = 1.7, respectively. These results suggest that the electrocatalysis of ORR by both Fe_2O_3/GCE and Co_3O_4/GCE is dominated by a 2-electrons transfer process to produce H_2O_2. In literature,[11,52,53] there is some difference in ORR electron transfer numbers, either 2-electron or 4-electron transfer processes.

To further investigate the ORR kinetics, the Tafel slopes of the steady-state polarization curves for Fe_2O_3/GCE and Co_3O_4/GCE (Figure 8) at the rotation rate of 300 rpm were obtained, and also corrected for ORR mass transport. According to equation 7, the term "$[(I_d \times I) / (I_d - I)]$" refers to the kinetic current density I_k of the ORR process. This current density is a result of the charge transfer process occurring between the surface of the catalyzed electrode and the solution oxygen, free of any mass transport effect. For Fe_2O_3/GCE, the Tafel slope obtained was 0.175 V dec^{-1}, while for Co_3O_4/GCE, the slope was 0.275 V dec^{-1}. These results indicate that Fe_2O_3/GCE is more favored than GCE/Co_3O_4 in terms of their catalytic ORR activities. The other possible reason may be the larger surface area of Fe_2O_3/GCE compared to that of Co_3O_4. Regarding Fe_2O_3/GCE ORR catalysis, Fu *et al.*[49] carried out a study

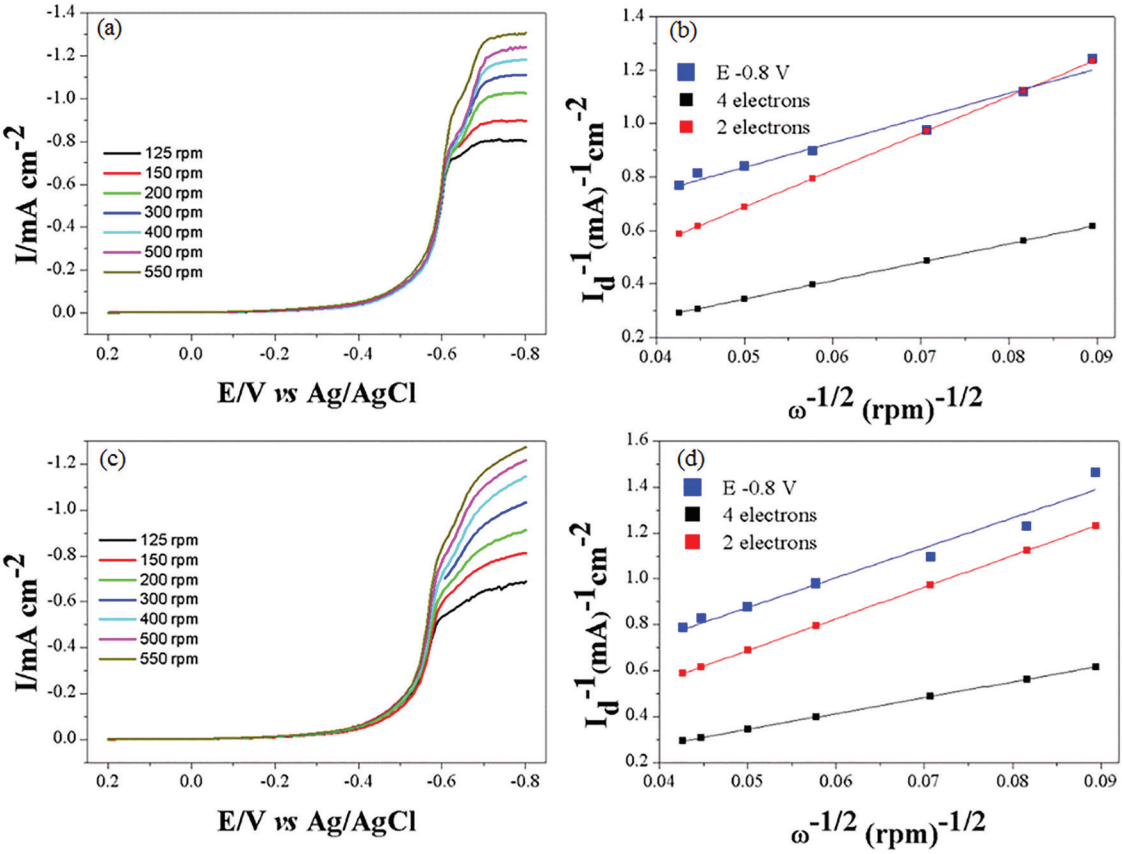

Figure 7. (a) ORR LSV curves recorded on Fe_2O_3/GCE in O_2-saturated BR buffer (pH = 1.8) at different electrode rotation rates from 125 to 550 rpm; (b) Koutecky-Levich (K-L) plots for Fe_2O_3/GCE based on the data of (a); (c) ORR LSV curves for Co_3O_4/GCE under the same conditions as (a); (d) K-L plots based on the data of (c). Potential scan rate: 5 mV s^{-1}.

with different forms of nanoparticle iron oxides (α-Fe_2O_3, α-Fe_2O_3-PPy and α-Fe_2O_3-C-N), and their Tafel slopes are similar to our results. Regarding Co_3O_4/GCE ORR catalysis, Liang *et al.*[54] compared two electrodes (Co_3O_4/N-rmGO and Co_3O_4/rmGO), showing that the Co_3O_4/N-rmGO electrode presented a lower Tafel slope, resulting in a higher catalytic activity.

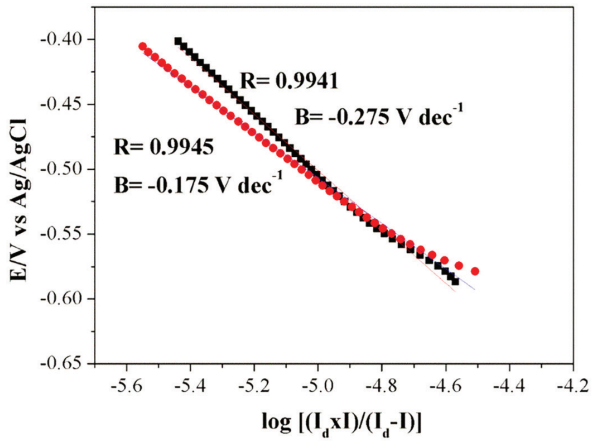

Figure 8. Tafel diagrams of ORR catalyzed by Fe_2O_3/GCE (red circle line) and Co_3O_4/GCE (black square line). Data extracted from the curve at 300 rpm of Figure 7.

Catalytic ORR current as a function of oxygen concentration

Figure 9 shows the linear sweep voltammograms (LSVs) of Fe_2O_3/GCE and Co_3O_4/GCE in the presence of different oxygen concentrations. It can be observed that for both electrodes the electrocatalytic currents increased with increasing oxygen concentration in the test cell. From the CVs, plots of log (I_p) *vs.* log [O_2] (Figures 9b and 9d) were obtained, which showed linear dependencies in the O_2 concentration range of 2.7×10^{-4} to 1.21×10^{-3} mol L^{-1}. This result suggests that Fe_2O_3 or Co_3O_4 modified GCE electrodes can be used for analysis of O_2 concentration in aqueous solution.

Conclusions

The electrochemically catalyzed oxygen reaction (ORR) is one of the most important reactions in many applications, particularly in fuel cells[2] and metal-air batteries.[1] However, the currently practical electrocatalysts are mainly based on precious metals (Pt, Pd, Ir, etc.), which are high cost. The development of highly active, stable and efficient, and cost effective

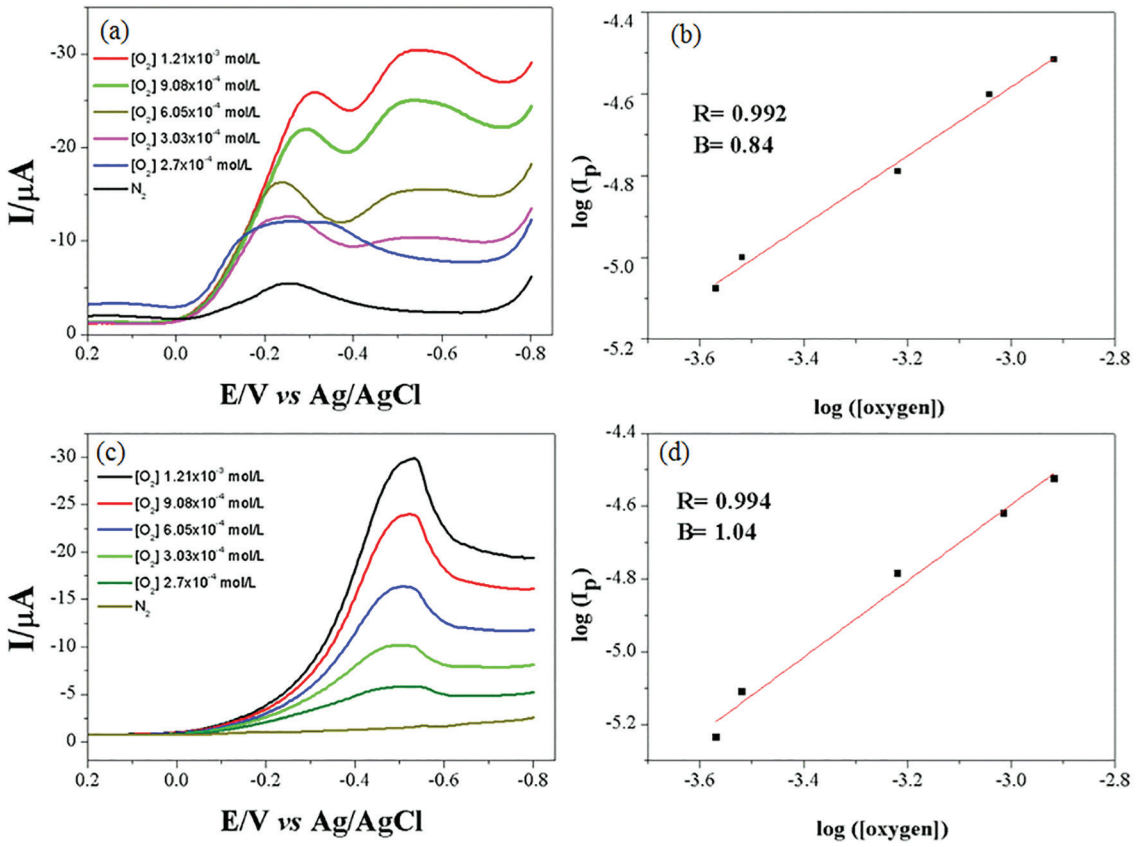

Figure 9. (a) LSVs at different oxygen concentrations for Fe_2O_3/GCE; (b) dependency of the logarithm I_p *vs*. the logarithm O_2 concentration [O_2] for Fe_2O_3/GCE; (c) Co_3O_4/GCE LSVs under the same conditions as (a); (d) dependency of the logarithm I_p *vs*. the logarithm [O_2] for Fe_2O_3/GCE.

non-precious metal electrocatalysts is therefore needed. In this paper, two non-noble metal catalysts, Fe_2O_3 and Co_3O_4 nanoparticles, were synthesized using the modified polymeric precursor method (Pechini). These two nanomaterials were characterized by Fourier transform infrared spectroscopy (FTIR) and X-ray diffraction (XRD) techniques for their compositions and crystal structures. The estimated average particle sizes were 21 and 31 nm for Fe_2O_3 and Co_3O_4, respectively. For characterizing the electrochemical activities, these two catalysts were individually employed to coat glass carbon electrodes for catalytic oxygen reduction reaction (ORR). Both cyclic voltammetry and rotating disc electrode (RDE) methods were employed to test the ORR activities of these catalysts. In particular, using RDE data and Koutecky-Levich theory, the results obtained indicate that both Fe_2O_3/GCE and Co_3O_4/GCE can catalyze ORR with a dominating 2-electron transfer process to produce H_2O_2. The electrochemical impedance spectroscopy was also used to obtain the charge transfer resistances of the ORR catalyzed by these two catalysts. In addition, the ORR Tafel slope for Fe_2O_3/GCE is lower than that of Co_3O_4/GCE, indicating that the former is more active than the latter. For fundamental understanding, the surface reaction processes on the electrode as well as their catalyzed ORR mechanisms are explored based on the experimental data and literature.

The result also shows a linear behavior between the catalytic current and the oxygen concentration, which suggests that these Fe_2O_3/GCE and Co_3O_4/GCE can be used as modified electrodes for analysis of O_2 concentration.

Overall, the results show that the nanoparticles of both Fe_2O_3 and Co_3O_4 have good catalytic activities toward ORR, but the former is more efficient than that the latter. Considering the low cost of these two non-noble metal catalysts, they may be used as viable alternatives for ORR electrocatalysts.

Acknowledgments

The authors are grateful to CNPq (PQ 2017, Process 310664/2017-9), FINEP (Research Project RECOL 05/ Subproject NANOPET), ANP (Research Project PMQC/ BIOPETRO, No. 1.029/2016-ANP-007.639), and CAPES for the financial support and fellowships received.

References

1. Wang, Y. J.; Fang, B.; Zhang, D.; Li, A.; Wilkinson, D. P.; Ignaszak, A.; Zhang, L.; Zhang, J.; *Electrochem. Energy Rev.* **2018**, *1*, 1.
2. Wang, R.; Wang, H.; Luo, F.; Liao, S.; *Electrochem. Energy Rev.* **2018**, *1*, 324.
3. Zhang, L.; Niu, J.; Dai, L.; Xia, Z.; *Langmuir* **2012**, *28*, 7542.
4. Ren, C.; Li, H.; Li, R.; Xu, S.; Wei, D.; Kang, W.; Wang, L.; Jia, L.; Yang, B.; Liu, J.; *RSC Adv.* **2016**, *6*, 33302.
5. Bezerra, C.; Zhang, L.; Lee, K.; Liu, H.; Marques, A.; Marques, E.; Wang, H.; Zhang, J.; Marques, A. L. B.; *Electrochim. Acta* **2008**, *53*, 4937.
6. Dias, V.; Fernandes, E.; da Silva, L.; Marques, E.; Zhang, J.; Marques, A.; Marques, A. L. B.; *J. Power Sources* **2005**, *142*, 10.
7. Costa, W. M.; Cardoso, W. S.; Marques, E. P.; Bezerra, C. W.; Ferreira, A. A. P.; Song, C.; Zhang, J.; Marques, A. L.; *J. Braz. Chem. Soc.* **2013**, *24*, 651.
8. Tian, N.; Lu, B. A.; Yang, X. D.; Huang, Y. H.; Huang, R.; Jiang, Y. X.; Zhou, Z. Y.; Sun, S. G.; *Electrochem. Energy Rev.* **2018**, *1*, 54.
9. Cardoso, W. S.; Dias, V. L.; Costa, W. M.; Rodrigues, I. A.; Marques, E. P.; Sousa, A. G.; Boaventura, J.; Bezerra, C. W. B.; Song, C.; Liu, H.; Zhang, J.; Marques, A. L. B.; *J. Appl. Electrochem.* **2009**, *39*, 55.
10. Higgins, D.; Zamani, P.; Yu, A.; Chen, Z.; *Energy Environ. Sci.* **2016**, *9*, 357.
11. Wu, Z. S.; Yang, S.; Sun, Y.; Parvez, K.; Feng, X.; Müllen, K.; *J. Am. Chem. Soc.* **2012**, *134*, 9082.
12. Chen, Z.; He, D.; Xu, X.; Liu, Z.; Huang, M.; Wang, X.; Jiang, H.; *RSC Adv.* **2016**, *6*, 34159.
13. Karunagaran, R.; Coghlan, C.; Tung, T. T.; Kabiri, S.; Tran, D. N.; Doonan, C. J.; Losic, D.; *New J. Chem.* **2017**, *41*, 15180.
14. Wang, Q.; Hu, W.; Huang, Y.; *Int. J. Hydrogen Energy* **2017**, *42*, 5899.
15. Xu, J.; Yang, H.; Fu, W.; Du, K.; Sui, Y.; Chen, J.; Li, M.; Zou, G.; *J. Magn. Magn. Mater.* **2007**, *309*, 307.
16. Epherre, R.; Duguet, E.; Mornet, S.; Pollert, E.; Louguet, S.; Lecommandoux, S.; Schatz, C.; Goglio, G.; *J. Mater. Chem.* **2011**, *21*, 4393.
17. Lima, S. A. M.; Sigoli, F. A.; Davolos, M. R.; Jafelicci, M. J.; *J. Alloys Compd.* **2002**, *344*, 280.
18. Silva, R. F.; Zaniquelli, M. E. D.; *Thin Solid Films* **2004**, *449*, 86.
19. Ren, S.; Ma, S.; Yang, Y.; Mao, Q.; Hao, C.; *Electrochim. Acta* **2015**, *178*, 179.
20. Sun, X.; Zheng, C.; Zhang, F.; Yang, Y.; Wu, G.; Yu, A.; Guan, N.; *J. Phys. Chem. C* **2009**, *113*, 16002.
21. Mirzaei, A.; Janghorban, K.; Hashemi, B.; Bonyani, M.; Leonardi, S. G.; Neri, G.; *Ceram. Int.* **2016**, *42*, 6136.
22. Gunnewiek, R. F. K.; Mendes, C. F.; Kiminami, R. H. G. A.; *Adv. Powder Technol.* **2016**, *27*, 1056.
23. Gharagozlou, M.; *J. Alloys Compd.* **2009**, *486*, 660.
24. Davis, J. C. In *Chemistry and Physics of Aqueous Gas Solutions*; Adams, W. A.; Greer, G.; Kell, G. S.; Desnoyers, J. E.; Oldham, K. B.; Atkinson, G.; Walkley, J., eds.; The Electrochemical Society: Princeton, NJ, USA, 1975, p. 393.
25. Chaves, J. A. P.; Araújo, M. F. A.; Varela, J.; Tanaka, A. A.; *Ecletica Quim.* **2003**, *28*, 2.
26. Ju, H.; Shen, C.; *Electroanalysis* **2001**, *13*, 789.
27. Cornell, R. M.; Schwertmann, U.; *The Iron Oxides: Structure, Properties, Reactions, Occurences and Uses*, 2nd ed.; Wiley: Weinheim, 2003.
28. Suresh, R.; Prabu, R.; Vijayaraj, A.; Giribabu, K.; Stephen, A.; Narayanan, V.; *Synth. React. Inorg., Met.-Org., Nano-Met. Chem.* **2012**, *42*, 303.
29. Bashir, S.; Mccabe, R. W.; Boxall, C.; Leaver, M. S.; Mobbs, D.; *J. Nanopart. Res.* **2009**, *11*, 701.
30. Eigler, S.; Dotzer, C.; Hirsch, A.; Enzelberger, M.; Müller, P.; *Chem. Mater.* **2012**, *24*, 1276.
31. Sahoo, S.; Satpati, A. K.; *J. Electroanal. Chem.* **2017**, *801*, 416.
32. Wang, H. W.; Hu, Z. A.; Chang, Y. Q.; Chen, Y. L.; Zhang, Z. Y.; Yang, Y. Y.; Wu, H. Y.; *Mater. Chem. Phys.* **2011**, *130*, 672.
33. Kamali, K. Z.; Alagarsamy, P.; Huang, N. M.; Ong, B. H.; Lim, H. N.; *Sci. World J.* **2014**, DOI: 10.1155/2014/396135.
34. Cao, R. B.; Chen, X. Q.; Shen, W. H.; Long, Z.; *Mater. Lett.* **2011**, *65*, 3298.
35. Adekunle, A. S.; Ozoemena, K. I.; *Int. J. Electrochem. Sci.* **2010**, *5*, 1726.
36. Shahid, M. M.; Rameshkumar, P.; Basirun, W. J.; Juan, J. C.; Huang, N. M.; *Electrochim. Acta* **2017**, *237*, 61.
37. Xu, C.; Wang, X.; Zhu, J.; Yang, X.; Lu, L.; *J. Mater. Chem.* **2008**, *18*, 5625.
38. Yang, X.; Fan, K.; Zhu, Y.; Shen, J.; Jiang, X.; Zhao, P.; Li, C.; *J. Mater. Chem.* **2012**, *22*, 17278.
39. Scherrer, P.; *Nachr. Ges. Wiss. Goettingen, Math.-Phys. Kl.* **1918**, *2*, 98.
40. Bazrafshan, H.; Tesieh, Z. A.; Dabirnia, S.; Touba, R. S.; Manghabati, H.; Nasernejad, B.; *Powder Technol.* **2017**, *308*, 266.
41. Cepriá, G.; Usón, A.; Pérez-Arantegui, J.; Castillo, J. R.; *Anal. Chim. Acta* **2003**, *477*, 157.
42. Oswald, H. R.; Asper, R.; *Preparation and Crystal Growth of Materials with Layered Structures*; Lieth, R. M. A., ed.; Reidel: Dordrecht, 1977, p. 73.
43. Barbieri, E. M. S.; Lima, E. P. C.; Lelis, M. F. F.; Freitas, M. B. J. G.; *J. Power Sources* **2014**, *270*, 158.
44. Gupta, A. K.; Gupta, M.; *Biomaterials* **2005**, *26*, 3995.
45. Kozhina, G. A.; Ermakov, A. N.; Fetisov, V. B.; Fetisov, A. V.; Shunyaev, K. Y.; *Russ. J. Electrochem.* **2009**, *45*, 1170.
46. Nicholson, R. S.; Shain, I.; *Anal. Chem.* **1964**, *36*, 706.

47. Ribeiro, C. D. L.; Santos, J. G. M.; de Souza, J. R.; Pereira-da-Silva, M. A.; Paterno, L. G.; *J. Electroanal. Chem.* **2017**, *805*, 53.
48. Liang, Y.; Wang, H.; Diao, P.; Chang, W.; Hong, G.; Li, Y.; Gong, M.; Xie, L.; Zhou, J.; Wang, J.; Regier, T. Z.; Wei, F.; Dai, H.; *J. Am. Chem. Soc.* **2012**, *134*, 15849.
49. Fu, Y.; Wang, J.; Yu, H. Y.; Li, X.; Wang, H.; Tian, J. H.; Yang, R.; *Int. J. Hydrogen Energy* **2017**, *42*, 20711.
50. Sun, M.; Zhang, G.; Liu, H.; Liu, Y.; Li, J.; *Sci. China Mater.* **2015**, *58*, 683.
51. Bard, A. J.; Faulkner, L. R.; *Electrochemical Methods: Fundamentals and Applications*; Wiley: New York, 2001.
52. Wang, K.; Wang, R.; Li, H.; Wang, H.; Mao, X.; Linkov, V.; Ji, S.; *Int. J. Hydrogen Energy* **2015**, *40*, 3875.
53. Mao, S.; Wen, Z.; Huang, T.; Hou, Y.; Chen, J.; *Energy Environ. Sci.* **2014**, *7*, 609.
54. Liang, Y.; Li, Y.; Wang, H.; Zhou, J.; Wang, J.; Regier, T.; Dai, H.; *Nat. Mater.* **2011**, *10*, 780.

Submitted: January 31, 2019
Published online: August 19, 2019